Published in final edited form as:
Cytoskeleton (Hoboken). 2013 June ; 70(6): 317–327. doi:10.1002/cm.21108.

Biochemical Evidence that Human EB1 Does not Bind Preferentially to the Microtubule Seam

Emily O. Alberico[1], **Daniel F. Lyons**[2], **Ryan J. Murphy**[1], **Julia T. Philip**[1], **Aranda R. Duan**[1], **John J. Correia**[2], and **Holly V. Goodson**[1,*]

[1]Department of Chemistry and Biochemistry, University of Notre Dame, Notre Dame, Indiana

[2]Department of Biochemistry, University of Mississippi Medical Center, Jackson, Mississippi

Abstract

EB1 is a highly conserved microtubule (MT) plus end tracking protein (+TIP) involved in regulating MT dynamics, but the mechanisms of its effects on MT polymerization remain undefined. Resolving this question requires understanding how EB1 interacts with MTs. Previous electron microscopy of the *S. pombe* EB1 homolog Mal3p suggested that Mal3p binds specifically to the MT seam, implying that EB1 family members promote MT polymerization by stabilizing the seam. However, more recent electron microscopy indicates that Mal3p binds everywhere except the seam. Neither set of experiments investigated the behavior of human EB1, or provided an explanation for why these studies arrived at different answers. To resolve these questions, we have used a combination of MT-binding assays and theoretical modeling with MTBindingSim. Our results indicate that human EB1 binds to the lattice, consistent with the recent Mal3p results, and show that Mal3p-binding assays that were previously interpreted as evidence for preferential seam binding are equally consistent with weak lattice binding. In addition, we used analytical ultracentrifugation to investigate the possibility that the EB1 monomer–dimer equilibrium might contribute to EB1 binding behavior, and determined that the EB1 dimerization dissociation constant is approximately 90 nM. We and others find that the cellular concentration of EB1 is on the order of 200 nM, suggesting that a portion of EB1 may be monomeric at physiological concentrations. These observations lead us to suggest that regulation of EB1 dimerization might play a role in controlling EB1 function.

Keywords

cytoskeleton; plus end tracking proteins; dimerization; tubulin; analytical ultracentrifugation

Introduction

Microtubules (MTs) are hollow polymeric tubes composed of α- and β-tubulin which are essential for processes including cell division and long-range intracellular transport. MTs

*Address correspondence to: Holly V. Goodson, 251 Nieuwland Science Hall, Notre Dame, Indiana 46556. hgoodson@nd.edu.

Additional Supporting Information may be found in the online version of this article.

also control cell polarity and cell motility [Desai and Mitchison, 1997; Howard and Hyman, 2003; Amos and Schlieper, 2005; Lansbergen and Akhmanova, 2006]. Typical MTs are composed of ~ 13 tubulin protofilaments laterally associated into a cylindrical lattice that close at a seam (Fig. 1a red arrow). The MT seam has different chemistry than the rest of the lattice because this is the only location where α-tubulin is adjacent to β-tubulin [Desai and Mitchison, 1997; Amos and Schlieper, 2005]. The tubulin interactions at the seam are thought to be weaker than the interactions at the lattice, although there is evidence that suggests otherwise [Simon and Salmon, 1990; Sui and Downing, 2010].

Due to the unique chemistry of the seam and the idea that the seam is a point of weakness in the MT structure, one might predict the existence of proteins that bind to and stabilize the seam [Simon and Salmon, 1990]. One protein that has been proposed to influence MT dynamics by binding to the seam is the MT plus end tracking protein (+TIP) EB1 [Sandblad et al., 2006]. EB1 is a highly conserved MT-binding protein that promotes MT polymerization and facilitates the binding of other proteins to the MT plus end [Akhmanova and Steinmetz, 2008]. It is thought that the active form of EB1 is the EB1–EB1 homodimer [Slep and Vale, 2007]. Because EB1 is a central component of the +TIP network and is a key regulator of MT dynamics, it is important to determine how it interacts with MTs. Therefore, there was great interest when studies using the *S. pombe* EB1 homolog Mal3p provided evidence that Mal3p binds to the MTs at the seam [Sandblad et al., 2006]. More specifically, electron microscopy of complexes formed between Mal3p and MTs showed the Mal3p binding in a line along the MT length that suggested binding to the seam, and cosedimentation assays were interpreted as showing that Mal3p saturated the MTs at a 1:9 ratio, similar to the 1:13 ratio expected for strong binding specifically to the MT seam [Sandblad et al., 2006]. However, more recent electron microscopy of complexes formed between Mal3p and GTP-γ-S MTs indicated that Mal3p binds everywhere except the seam [Maurer et al., 2011, 2012].

These experiments left several issues unresolved, including how human EB1 behaves, and why these studies arrived at different results. To address these questions, we used a combination of mathematical modeling and MT-binding experiments. These data lead us to conclude that binding of human EB1 to stabilized MTs does not occur predominantly at the MT seam. At moderate concentrations of EB1 (2–4 μM), our data are most consistent with simple, weak binding to the MT lattice. However, at lower concentrations of EB1 (1 μM), we observed small deviations from the expected binding behavior that were within error but could potentially be accounted for by dissociation of some EB1 dimers into monomers. To test this hypothesis, we used analytical ultracentrifugation (AUC) to investigate the EB1 monomer–dimer equilibrium, and found that under buffer conditions similar to those used in the MT-binding experiments, the K_d for dimerization of full-length EB1 is approximately 90 nM. Including this dimerization process resulted in a binding model that fits the data slightly better. More significantly, since EB1 monomer binds to MT tips and lattice much more weakly than does the dimer [Slep and Vale, 2007; Skube et al., 2011], the proximity of this K_d to the estimated concentration of EB1 in cytosol [Tirnauer et al., 2002; Katsuki et al., 2009] raises the possibility that dimerization is involved in the regulation of EB1 function.

Results and Discussion

To determine whether human EB1 binds preferentially to the MT seam, we took a two-pronged approach: we first used theoretical models to identify experiments that should distinguish between seam-only and lattice binding, and then tested our models through EB1–MT binding experiments. Because a given concentration of typical MTs has 1/13th as many seam binding sites as lattice-binding sites, we expected that the most straightforward way to distinguish between the seam-only and lattice-binding models would be to examine how the fraction of EB1 bound to MTs changes as a function of EB1 concentration.

To computationally simulate the different behaviors expected from lattice binding and seam-only binding at various EB1 concentrations, we used MTBindingSim, a freely-available program that allows one to explore the expected binding behavior under a range of binding models, experimental designs, and conditions [Philip et al., 2012]. More specifically, for each possible binding model, the program allows you to input postulated K_d values for each interaction, the concentration (or concentration ranges) for each binding partner, the experimental design (e.g., changing the concentration of MTs or MT-binding protein), and the approach to presenting the data (e.g., plotting the binding as a function of MT_{Free} concentration or MT_{Total} concentration).

To begin, we wanted to see how various theoretical binding models fit the existing data used to support binding of Mal3p to the MT seam. To do this, we extracted estimates of the binding data as presented in Sandblad et al. [2006] (Fig. 1b). According to the original interpretation in their manuscript, the binding of Mal3p to MTs reaches a maximum at ~ 18 μM MTs, which corresponds to a 1:9 Mal3:tubulin dimer ratio and is close to the ~ 1:13 ratio expected for seam-only binding under the assumption that the MTs have 13 protofilaments [Sandblad et al., 2006] (Fig. 1b). However, it is important to point out that under this interpretation, maximum Mal3p binding occurs with only 60% of the Mal3p bound, which would imply that only ~60% of the Mal3p is active. By eye, it seemed likely that the data could be equally well-explained by assuming that all of the Mal3p is active, and that it simply binds weakly all along the lattice (Fig. 1b). To investigate this possibility more rigorously required theoretical modeling. Below, we first use these models to investigate human EB1, and then return to Mal3p.

Seam-Only Binding Model

In this model, the simulation assumes that the binding protein (i.e., EB1) binds to the seam with one value, $K_{d\text{-}S}$ and to the lattice with another value, $K_{d\text{-}L}$. For the purpose of designing experiments that would be able to distinguish between strong binding to the seam and weak binding to the lattice, we needed to find a $K_{d\text{-}S}$ value that fit the existing EB1–MT binding data. We chose to perform our experiments with the “activated” form of EB1 termed $EB1_{248}$ (Fig. 1c) because the full length protein ($EB1_{FL}$) contains an acidic autoinhibitory tail that binds to the head domain and “turns off ” the binding of EB1 to MTs [Hayashi et al., 2005; Zhu et al., 2009]. This autoinhibition is relieved in vivo through binding of other proteins such as p150 or Adenomatous Polyposis Coli (APC) [Hayashi et al., 2005; Slep et al., 2005]. We chose to use $EB1_{248}$ to mimic MT binding in vivo where other proteins are present to relieve autoinhibition.

To simulate preferential seam-only binding as it should occur at different values of $K_{d\text{-}S}$ in the absence of significant lattice binding, we set the $K_{d\text{-}L}$ value to 10^6 μM (i.e., no binding to the lattice), set the EB1 concentration to 2 μM (similar to published MT-binding assays with $EB1_{248}$ [Zhu et al., 2009], and varied the values for the seam affinity ($K_{d\text{-}S}$). We then plotted fractional EB1 saturation as a function of total polymerized tubulin (MT_{Total}) concentration for a series of different $K_{d\text{-}S}$ values (Supporting Information Fig. S1a), and compared these curves to the existing $EB1_{248}$ binding data [Zhu et al., 2009]. This preliminary analysis (not shown, but see Fig. 3 below) suggested that a $K_{d\text{-}S}$ value of 1 μM was consistent with the existing experimental data on $EB1_{248}$–MT interactions and would be a good foundation for designing experiments.

To see how the binding curves as predicted by the seam-only binding model change if the EB1 concentration is varied, we ran simulations where the concentration of EB1 was changed from the original 2 μM to 4 μM or 1 μM. We observed that with the seam-only binding model, the predicted binding curves shift significantly down and to the right as the concentration of EB1 is increased from 1 μM to 2 μM and 4 μM (Fig. 2a). The curves shift down as EB1 concentration increases because a significant fraction of the binding sites are occupied by EB1 over the entire range of MT concentrations considered. When more EB1 molecules compete for the same number of binding sites, the fraction of total EB1 that is bound at a given MT concentration falls[1]. The shift in the fraction of EB1 bound is particularly clear when the data for 15 μM MTs are represented as a bar graph (Fig. 2b).

Lattice-Binding Model

In this model, the simulation assumes that EB1 binds anywhere on the MT surface with a single K_d value. Supporting Information Fig. S1b shows how the fraction of EB1 bound at different concentrations of polymerized tubulin should change with the K_d under the assumption that EB1 binds to MTs according to the lattice-binding model. Note that much more EB1 is bound at a given K_d and MT_{Total} concentration in Supporting Information Fig. S1b than in Supporting Information Fig. S1a because there are many more lattice-binding sites than seam binding sites.

To see how the binding curves as predicted by this lattice model change when the EB1 concentration is varied, we set the lattice-binding affinity to 13 μM because this is the $K_{d\text{-}L}$ value that best fits our preliminary experiments with 2 μM $EB1_{248}$ (not shown), and it is similar to the previously reported lattice K_d value of 10 μM for 2 μM $EB1_{248}$ [Zhu et al., 2009]. We then ran simulations parallel to those performed for the seam-only binding model, that is, we increased the EB1 concentration from 1 μM to 2 μM to 4 μM. Under these conditions, we found that the theoretical binding curves do not change between 1 μM and 4 μM EB1 (Fig. 2c), in contrast to the shift that is predicted for the seam-only binding model (compare Fig. 2a to Fig. 2c). The superposition of the predicted curves for the lattice-

[1]In interpreting these behaviors, it is important to remember that we are plotting the fraction of EB1 bound as a function of MT_{Total} concentration, i.e., the total concentration of MTs present in the assay. If we had plotted the data as a function of MT_{Free} concentration, the curves would not shift, i.e., the fraction of EB1 bound to MTs at a given MT_{Free} concentration would not vary with EB1 concentration. We have chosen to plot the data as a function of MT_{Total} concentration because in experiments one needs to make assumptions about the binding ratio in order to calculate MT_{Free} concentration, and it is the binding ratio that we are trying to investigate.

binding model occurs because most of the MT sites remain unoccupied even at the higher concentrations of EB1. This means that as the concentration of EB1 increases, the fraction of EB1 able to bind at a given MT_{Total} concentration remains constant. The difference in predicted binding behaviors for the seam-only and lattice-binding models is particularly apparent at 15 μM MTs (compare Figs. 2b and 2d).

In summary, the simulations predict that if EB1 is binding primarily to the seam, the binding curve should shift significantly to the right as EB1 concentration is changed from 1 μM to 2 μM to 4 μM. In contrast, if EB1 is binding to the lattice, the binding curves should remain unchanged as the concentration of EB1 is varied between 1 μM, 2 μM, and 4 μM.

Simulating the Behavior of Mal3p

As noted above, visual examination of the Sandblad et al. [2006] data (Fig. 1b) suggested that while it was interpreted as supporting seam-only binding, it is also consistent with weak lattice binding. To test this hypothesis, we used MTBindingSim as above. Figure 1b shows that both models are indeed consistent with the Sandblad et al. [2006] data. More specifically, the seam binding model is consistent with the data when it has a strong $K_{d\text{-}S}$ (~0.001 μM) and only ~60% active protein, while the lattice-binding model is consistent with the data when it has a weak $K_{d\text{-}L}$ (~10 μM) and 100% active protein.

Experimental Tests and Comparison to the Predicted Binding Behavior

To conduct experimental tests and compare the data to our two binding models, we first determined the binding behavior of varied concentrations of $EB1_{248}$ at 15 μM MTs, since this is the concentration of MTs at which the models predict a significant difference between seam-only and lattice binding (compare Figs. 2b and 2d). We found that 2 and 4 μM $EB1_{248}$ have almost identical fraction bound values (Fig. 3a). This observation is consistent with the predictions for the lattice model (Fig. 2d) and inconsistent with the predictions for the seam-only model (Fig. 2b), arguing against the idea that human EB1 binds to the seam. However, we noted that 1 μM $EB1_{248}$ bound less than anticipated with either model. This deviation is not statistically significant, but it raised the possibility that an additional interaction not incorporated into these either model might be occurring (Fig. 3a).

To further test our models, we performed full binding studies (separate from the initial studies performed above) in which we varied MTs from 0 to 25 μM and held $EB1_{248}$ constant at 1, 2, or 4 μM (Supporting Information Figs. S2a–S2c). We then superimposed the averaged data on to the predicted lattice-binding curves (Fig. 3b) or the predicted seam-only binding curves (Fig. 3c). Our first observation from these data was that these more in-depth experiments were also inconsistent with the seam-only binding model: while the seam-only binding model predicts that the curves should shift to the right as the concentration of EB1 is increased, we found instead that the curves for higher concentrations of $EB1_{248}$ largely superimposed on those for the lower concentrations, with no evidence for a shift to the right at higher EB1 concentrations. These data strongly argue against the idea that human EB1 binds preferentially to the MT seam. The 1 μM full binding data again deviated slightly from predicted binding behavior when compared to the higher

concentrations of EB1 (2 and 4 μM) although this deviation was within the error of the dataset.

One might raise the question of whether either model would be more consistent with the data if the assumed K_d values were changed. Stronger seam binding would predict that a significantly larger fraction of 1 μM EB1 would be bound at 25 μM MTs, while weaker seam-only binding would predict that less EB1 is bound at 25 μM MTs (Supporting Information Fig. S1a).

Because all of our experiments were conducted with the activated EB1 fragment $EB1_{248}$, we wanted to verify that $EB1_{FL}$ (the form of EB1 present in vivo) behaves similarly to $EB1_{248}$. To do this, we first determined the predicted binding behavior of varied concentrations of $EB1_{FL}$ (1, 2, and 4 μM) at 15 μM MTs under the seam-only model and the lattice model (Supporting Information Figs. S3a and S3b, respectively) and then compared these predictions to experimental observations (Supporting Information Fig. S3c). We found that the $EB1_{FL}$ binding data also rule out strong seam binding because the data do not show the expected decrease in fraction $EB1_{FL}$ bound predicted under this model (compare Supporting Information Figs. S3a–S3c). Therefore, we conclude that our binding data for both $EB1_{FL}$ and $EB1_{248}$ are inconsistent with the idea that EB1 binds with strong preference for the MT seam.

We wanted to return to observations mentioned above that the 1 μM $EB1_{248}$ data deviated slightly from the lattice-binding predictions: in both Figs. 3a and 3b, the 1 μM $EB1_{248}$ appeared to bind slightly more weakly than did 2 μM or 4 μM $EB1_{248}$. If EB1 is binding according to a simple lattice-binding model, the K_d values should not depend on the concentration of EB1. Although these deviations were within error, we thought that it was worthwhile to consider the possibility that dissociation of EB1 into monomers might be affecting its MT-binding behavior. The monomer form of EB1 binds to the MT much more weakly than does the dimer [Slep and Vale, 2007; Skube et al., 2011]. The K_d for the EB1–EB1 interaction has been reported to be less than 1 μM although the exact number has not been determined [De Groot et al., 2010; Skube et al., 2011].

To resolve the question of whether including EB1 dimerization into our binding model would improve the fit of the data, we set out to determine the dimerization K_d experimentally using AUC. We began by analyzing the purity, stability, and hydrodynamic properties of $EB1_{248}$ using sedimentation velocity (SV) from 2.31 μM to 25.98 μM (Supporting Information Fig. S5A) at 20°C. The data indicated that the samples were pure and stable over the time course of the experiment. Global analysis of the raw SV data using SedAnal [Stafford and Sherwood, 2004] suggested that the predominant species was an EB1 dimer with approximately 3% aggregate (predominantly a dimer–dimer). At 2.31 μM, there appeared to be a small centripetal (smaller s) shift that suggested a slight dissociation into monomers. Attempts to explore this by fluorescently labeling $EB1_{248}$ were unsuccessful due to low labeling efficiency, low signal/noise, and inconsistent results (data not shown).

The $EB1_{248}$ was then analyzed using sedimentation equilibrium where nine samples spanning a concentration range from 1 to 10 μM were centrifuged until equilibrium was

reached at 21K, 25K, and 28K rpm at 20°C (Supporting Information Fig. S6). Global analysis of all 27 datasets suggested a slight decrease in the weight average MW, or increase in K_d when fit to a reversible dimerization model, of the samples with increasing velocity, suggesting that the system was dissociating at low concentrations into monomer (Supporting Information Table S2). The SE experiment was then repeated at 30°C and 35°C. During both experiments, the system displayed a very slow approach to equilibrium at 25 K and 28 K (data not shown). The weight average MW during both experiments decreased at 28 K to significantly below the MW of $EB1_{248}$ monomer. We therefore repeated a SV experiment at 35°C to explore this decrease in stability and observed extensive aggregation (data not shown). These experiments suggest that in dilute conditions and high temperatures that EB1 dimer is not stable over the time course of a typical SE experiment (approximately four days). This also suggests that the slight centripetal shift observed in the SV data at 2.31 μM could be attributed to slight degradation, rather than dissociation.

It was then decided to repeat the analyses at a lower temperature in order to stabilize the protein over the time course of the experiment and also to use $EB1_{FL}$ in order to improve the signal (as a reminder, all experiments above used the activated fragment $EB1_{248}$; the full length construct has a higher extinction coefficient and is therefore preferable for analyses at lower concentrations). First, the SV analysis was performed with $EB1_{FL}$ at 20°C from 6.51 μM to 27.74 μM (Supporting Information Fig. S5B). The sample was determined to be pure and stable over the time course of the experiment. Global analysis suggested that, similar to the truncated $EB1_{248}$, the predominant species sedimented at an s value consistent with $EB1_{FL}$ dimer and approximately 3% aggregate (predominantly a dimer–dimer). The small centripetal (smaller s) shift seen in Supporting Information Fig. S5A was not observed. SE was then performed using the same experimental procedure in the earlier SE analysis, only lowering the temperature to 4°C and using $EB1_{FL}$ (Fig. 4). Analysis of the data suggested a slight decrease in weight average MW that is consistent with dissociation into monomer. This decrease was attributed to dissociation, and not instability, since there was no problem when the system was approaching equilibrium. Fitting the data to a reversible dimerization model produced a K_d of 88.5 nM (24 nM, 196 nM) (best fit [68% confidence interval]; see Supporting Information Table S3).

To investigate the impact of dimerization on EB1–MT binding in our assays, we used MTBindingSim and set the K_d values as follows: (a) the K_d for EB1 dimer–MT interaction was set to 13 μM (Supporting Information Fig. S2); (b) the K_d for EB1 monomer–MT interaction was set to 100 μM (estimated from unpublished data); and (c) the K_d for the EB1–EB1 dimerization was set to 90 nM (obtained from the AUC). We found that with a dimerization K_d of 90 nM, the model does not predict an observable reduction in the binding of 1 μM EB1 (compare Fig. 3d inset to Fig. 3a). Instead, we found that reduced binding with 1 μM EB1 relative to 4 μM EB1 is predicted to become obvious only with a much weaker EB1 dimerization K_d, for example, 0.5–1 μM (not shown). However, although the difference is small, the theoretical curves generated with this model are more consistent with all three datasets than are the models that failed to take dimerization into account (Fig. 3d, compare to Figs. 3b and 3c, see also Supporting Information Table S1). Thus, these binding data are

consistent with the conclusion of the AUC analysis that the EB1 dimerization affinity is ~90nM.

To address the question of whether the EB1 monomer–dimer equilibrium might play a role in EB1 function in vivo, it is necessary to consider the concentration of EB1 in cytosol. The concentration of EB1 in vertebrate cytoplasm has previously been reported as ranging between 0.25 and 2 μM in Xenopus egg extract [Tirnauer et al., 2002; Kronja et al., 2009] and tens of nanomolar in *S. pombe* [Katsuki et al., 2009]. We estimated the concentration of EB1 in HeLa cells to be ~0.25 μM using quantitative western blots (Table I and Supporting Information Figs. S4a and S4b). Our measured K_d of 90 nM for the EB1–EB1 dimerization is near these values and suggests that while most of the EB1 in cytosol is likely dimeric, a portion of the EB1 present in cells may be in the monomeric form, though the exact monomer–dimer ratio is difficult to predict because of differences in buffer conditions and effects such as molecular crowding. Recently, Seetapun et al. [2012] concluded that EB1 exists primarily in dimer form in LLCPK1 epithelial cells, in agreement with these conclusions. However, it is interesting to consider the possibility that under some conditions, a shift in the EB1 monomer–dimer ratio could play a role in EB1 regulation, an issue that was also raised by De Groot et al. [2010]. It is intriguing to note that the EB1-binding proteins known to “turn on” EB1 are themselves dimers (e.g., CLIP-170, p150). The dimerization of EB1 would be enhanced by binding to these proteins and could act as a molecular switch to shift EB1 from an inactive (monomer) state to an active (dimer) state.

Finally, it is important to note that in vitro MT plus-end tracking (+TIP) experiments using EB1 are frequently performed at concentrations at or below 100 nM [e.g., Dixit et al., 2009; Maurer et al., 2012], suggesting that the EB1 monomer–dimer equilibrium could be contributing to EB1 behavior and activity in these assays. Much of the existing in vitro +TIP work has utilized the *S. pombe* EB1 homolog Mal3, which would likely have a different (perhaps stronger) dimerization affinity. However, the possibility that changes in EB1 concentration and/or the addition of EB1-binding proteins could alter the EB1 monomer/dimer ratio is something to consider in future work.

Conclusions

To understand EB1 and its role as the core of the +TIP network, it is important to establish how it interacts with MTs. As discussed above, recent publications focused on the *S. pombe* EB1 ortholog Mal3p yielded conflicting conclusions about whether Mal3p binds to the MT seam or to the MT lattice. We have used a combination of theoretical modeling and experimental binding assays to investigate the origin of this discrepancy and determine whether human EB1 binds primarily to the seam or lattice. First, our theoretical modeling shows that the biochemical data that were presented in Sandblad et al. [2006] and interpreted as evidence for strong binding to the MT seam are equally consistent with weak lattice binding, indicating that these data cannot be used to resolve the Mal3p-binding mechanism. Second, the combination of our modeling and binding assays indicate that human EB1 does not bind strongly to the MT seam and are consistent with the idea that EB1 binds weakly to the MT lattice. Similar results were obtained for both $EB1_{248}$ and $EB1_{FL}$. Putting these data

together with those of Maurer et al. [2012], we conclude that EB1 and its orthologs (including Mal3p) bind to the MT lattice and not to the seam.

To investigate the possibility that the EB1 monomer–dimer equilibrium might be contributing to the EB1-binding behavior, we used AUC, and observed that the $EB1_{FL}$ dissociation constant is approximately 90 nM under the conditions of our experiments. Comparison of this value to cytosolic concentrations of EB1 suggests that most EB1 is dimeric, consistent with recent measurements in vivo [Seetapun et al., 2012], but raises the possibility that modulation of EB1 dimerization through posttranslational modification or interaction with binding proteins might play a role in the regulation of EB1 activity and thus MT dynamics.

Materials and Methods

Protein Purification

$EB1_{FL}$ and $EB1_{248}$ were cloned and purified as previously described [Zhu et al., 2009]. Briefly, bacterial expressed $EB1_{FL}$ or $EB1_{248}$ were purified using sequential cation and anion exchange resins (DE52 and P11 Whattman at pH 7.9 and 6.8, respectively) eluted by increasing concentrations of NaCl (25–300 mM) followed by desalting on a PDG-6 resin and elution into PEM buffer (100 mM Pipes, 2 mM $MgCl_2$, 1 mM EGTA, pH 6.8). Protein concentration was determined by Bradford with BSA standard. Purified proteins were flash frozen and stored at −80°C.

Tubulin was purified as previously described [Zhu et al., 2009]; briefly tubulin was purified from porcine brain through two rounds of polymerization and depolymerization followed by purification on a P11 resin (Whattman pH 6.8). Tubulin concentration was measured by Bradford with BSA standard, flash frozen, and stored at −80°C. MTs were polymerized with Taxol (paclitaxel, Sigma Alrich) as previously described [Zhu et al., 2009]. MT concentration was measured by Bradford with BSA standard. Purified MTs were flash frozen and stored at −80°C.

Theoretical Binding Curves

Theoretical binding models were generated using MTBindingSim version 0.9 [Philip et al., 2012]. MTBindingSim is a freely available, open source program that can be found at www.BindingTutor.org. For all theoretical binding models generated, the concentration of EB1 was set to either 1 μM, 2 μM, or 4 μM and the binding ratio was set at 1 EB1:1 polymerized tubulin dimer on the seam or lattice as appropriate. $EB1_{248}$ Predictions: To generate the seam-only binding model, the $K_{d\text{-}L}$ for the EB1–lattice interaction was set to 100,000 μM and the $K_{d\text{-}S}$ for EB1–seam interaction was set to 1 μM using the “MT seam and lattice” binding model. To generate the lattice model, the K_d for EB1–lattice was set to 13 μM using the “first order” binding model. To generate the lattice with dimerization model, the dimer–lattice K_d was set to 13 μM and the monomer–lattice K_d was set to 100 μM under the “MAPs dimerize” binding model. The EB1–EB1 dimerization K_d was set to 90 nM, that is, the EB1 dimerization affinity measured by AUC. $EB1_{FL}$ Predictions: To generate the seam-only binding model, the $K_{d\text{-}L}$ for the EB1–lattice interaction was set to

100,000 μM and the $K_{d\text{-}S}$ for EB1–seam interaction was set to 1.5 μM using the "MT seam and lattice" binding model. Preliminary analysis (not shown) suggested that a $K_{d\text{-}S}$ value of 1.5 μM was consistent with the existing experimental data on $EB1_{FL}$–MT interactions. To generate the lattice model, the K_d for EB1–lattice was set to 20 μM using the "first order" binding model (the previously measured lattice K_d value [Zhu et al., 2009].

MT-Binding Experiments

Binding data were collected using cosedimentation assays as previously described [Zhu et al., 2009]. Various concentrations of MTs were incubated with either 1 μM, 2 μM, or 4 μM $EB1_{248}$ or $EB1_{FL}$ for 25 min at 37°C in the presence of 10 μM Taxol. The samples were spun down at 65,000 rpm in a tabletop ultracentrifuge for 15 min at 37°C. The supernatant was removed and the pellet was resuspended in PEM buffer. The supernatants and pellets were ran on a 10% SDS gel and stained with Comassie. The fraction of EB1 bound was determined by densitometry with ImageJ (NIH).

To extract an apparent K_d from these binding data, we used Prism 4.0 to fit the data to a standard bimolecular binding equation $Y = B_{max} * X/(K_d + X)$ where Y is the fraction EB1 bound, B_{max} is the maximal achievable binding (set to 1 assuming 100% active protein), and X is the concentration of free MTs, which was estimated from the concentration of bound EB1 assuming a 1:1 binding ratio. We assumed that 100% of our EB1 protein is active based on other experiments (not shown) in which we found that when we mixed the unbound fraction from one experiment with new MTs, they behaved similarly to the original EB1, and on the observation that only 3% of the EB1 in the AUC experiments was aggregated (not shown).

Quantitative Western Blots

HeLa cytosol (10.6 mg/ml) was diluted 5:1 into sample buffer. EB1 standards (0.025, 0.05, 0.1, 0.15, 0.2 μM final) were diluted into BSA (1.5 μM final for loading control and visualization) and sample buffer and run on a 10% SDS gel. The samples were transferred to a nitrocellulose membrane. The primary EB1 antibody (BD Bioscience Mouse Anti-EB1 antibody) and secondary antibody (Antimouse HRP Jackson ImmunoResearch) were used to visualize EB1. The intensity of the bands was quantified using ImageJ (NIH) and a standard curve was generated for each experiment. Three separate blots and standard curves were generated and quantified. Using this approach, we found that the concentration in diluted cytosol was 0.08 ± 0.004 μM. Given that the diluted cytosol concentration was found to be 10.6 mg/ml using Bradford, and that we assume that the cytosol was diluted 3x–4x during preparation, we estimate that the concentration of EB1 in undiluted cytosol (e.g., in cells) is between 0.2 and 0.3μM (e.g., ~.25μM).

AUC Experimental Procedure

Samples were prepared for AUC experiments by thawing an aliquoted freezer stock of EB1 at room temperature, then diluting to approximately 600 μL and taking an absorbance spectra to determine $EB1_{FL}$ or $EB1_{248}$ concentration. All AUC data was collected in a Beckman XL-A with an added fluorescence detection system (AVIV-FDS).

SV was performed by diluting the stock to the desired concentration with a volume of 550 μL (1.2 cm centerpieces) or 150 μL (3 mm centerpieces). These samples were loaded directly into SV centerpieces with a buffer sample to subtract the absorbance of the buffer. The temperature of the AUC was equilibrated to 20.0°C (corresponding to 19.7°C [Liu and Stafford, 1995]) until the temperature remained constant for at least 10 min. The samples were sedimented at 60,000 rpm and the sedimentation was monitored by observing the absorbance at 280 nm, 240 nm, or 233 nm with a spacing of 0.02 cm averaging four scans in continuous scan mode. The run was stopped when the concentration versus radial distance profiles stopped changing with time, indicating that the sample had fully sedimented. Fluorescein Isothiocyanate (FITC) and Alexa-488 labeled $EB1_{248}$ samples were run in the same way, with the exception that fluorescence data was averaged over five scans, no buffer blank was used, and after the sample had sedimented a pseudoabsorbance scan was taken at the same speed to determine the meniscus position.

Sedimentation Equilibrium (SE) (Fig. 4 and Supporting Information Fig. S6) was performed by diluting an $EB1_{FL}$ or $EB1_{248}$ stock as indicated to 150 μL volumes at the desired concentrations. The samples were then pipetted into six channel cells (110 μl sample and 120 μl of reference buffer). The angular velocities for the SE experiments were chosen by calculating Sigma values (reduced molecular weights) based on the EB1 AA sequence to equal ~3 (21,000 rpm), ~4 (25,000 rpm), and ~5 (28,000 rpm) using the software program SedNTerp [Laue et al., 1992]. The run was then set up for the corresponding speeds and scans set to be taken every 4 h at 280 nm with 0.001 cm spacing in step mode averaged over nine scans. The scans were taken from the AUC computer and imported into the software program WINMATCH [Cole et al., 2008] to determine if the system had reached equilibrium. Once the system was determined to have reached equilibrium, the velocity was increased to the next speed and allowed to reequilibrate.

AUC Analysis Procedure

SV data was analyzed using the following procedure. The meniscus position was determined by importing the raw data into DCDT 2+ [Philo, 2006] and using the software to determine the maximum peak height. The raw data was then imported into Sedfit [Schuck, 1998] and analyzed using a c(s) distribution from 0.1 to 10.01 S with a 0.1 S resolution. The area under the peak was integrated to determine the weight average sedimentation coefficient. If sufficient signal was present, the data were then analyzed in DCDT 2+ using a g(s) distribution to determine the weight average sedimentation coefficient. The weight average sedimentation coefficient was plotted versus the logarithm of [EB1] to construct a binding curve and estimate the association constant. If sufficient signal was present, the raw data was then imported into SedAnal [Stafford and Sherwood, 2004] and analyzed using global direct boundary fitting to both single species and reversible monomer–dimer models. Global direct boundary fitting to reversible association models was used to estimate association constants for the dimerization process. In all cases, absorbance and FDS, the data were consistent with a tight dimer that showed no significant dissociation (Supporting Information Fig. S5).

SE data (Fig. 4 and Supporting Information Fig. S6) was analyzed using the following procedure. The data was imported into SedAnal, preprocessed into nine different channels of data at each speed, and analyzed using global direct boundary fitting. The data was fit to both single species and reversible monomer–dimer models (refer to Supporting Information Fig. S4 and Table S2) and the latter was used to estimate an association constant for the dimerization. Error bars were estimated with Fstat using a target value according to Eq. 35 in Johnson and Straume [1994]. Note the slight drift in K_d with speed and thus time. This drift was also accelerated by elevated temperature, such that at 35°C the samples equilibrated very slowly (~30 h) and were all monomeric in the second and third speed. Thus, the global fits of all speeds provides an upper estimate of the K_d.

Supplementary Material

Refer to Web version on PubMed Central for supplementary material.

Acknowledgments

This work is supported by the National Science Foundation (grant 0951264 to H.V.G.). AUC experiments were conducted in the UMMC AUC Facility and supported by an NSF MRI grant (1040372 to JJC). We would like to thank the members of the Goodson lab for their insightful discussion and critique of this manuscript.

References

Akhmanova A, Steinmetz MO. Tracking the ends: a dynamic protein network controls the fate of microtubule tips. Nat Rev Mol Cell Biol. 2008; 9(4):309–322. [PubMed: 18322465]

Amos LA, Schlieper D. Microtubules and maps. Adv Protein Chem. 2005; 71(04):257–298. [PubMed: 16230114]

Cole JL, Lary JW, Moody TP, Laue TM. Analytical ultracentrifugation: sedimentation velocity and sedimentation equilibrium. Methods Cell Biol. 2008; 84(07):143–179. [PubMed: 17964931]

Desai A, Mitchison TJ. Microtubule polymerization dynamics. Annu Rev Cell Dev Biol. 1997; 13:83–117. [PubMed: 9442869]

De Groot CO, Jelesarov I, Damberger FF, Bjelić S, Schärer MA, Bhavesh NS, Grigoriev I, Buey RM, Wuthrich K, Capitani G, et al. Molecular insights into mammalian end-binding protein heterodimerization. J Biol Chem. 2010; 285(8):5802–5814. [PubMed: 20008324]

Dixit R, Barnett B, Lazarus J, Tokito M, Goldman Y, Holzbaur E. Microtubule plus-end tracking by CLIP-170 requires EB1. Proc Natl Acad Sci. 2009; 106(2):492–497. [PubMed: 19126680]

Hayashi I, Wilde A, Mal TK, Ikura M. Structural basis for the activation of microtubule assembly by the EB1 and p150Glued complex. Mol Cell. 2005; 19(4):449–460. [PubMed: 16109370]

Howard J, Hyman A. Dynamics and mechanics of the microtubule plus end. Nature. 2003; 422(6933): 753–758. [PubMed: 12700769]

Johnson, ML.; Straume, M. Modern Analytical Ultracentrifugation. Boston: Birkhäuser; 1994. Comments of the analysis of sedimentation equilibrium experiments; p. 37-65.

Katsuki M, Drummond DR, Osei M, Cross R. Mal3 masks catastrophe events in Schizosaccharomyces Pombe microtubules by inhibiting shrinkage and promoting rescue. J Biol Chem. 2009; 284(43): 29246–29250. [PubMed: 19740752]

Kronja I, Kruljac-Letunic A, Caudron-Herger M, Bieling P, Karsenti E. XMAP215-EB1 interaction is required for proper spindle assembly and chromosome segregation in *Xenopus* egg extract. Mol Biol Cell. 2009; 20:2684–2696. [PubMed: 19369422]

Lansbergen G, Akhmanova A. Microtubule plus end: a hub of cellular activities. Traffic. 2006; 7(5): 499–507. [PubMed: 16643273]

Laue, TN.; Shah, BD.; Ridgeway, TM.; Pelletier, SM. Computer-aided interpretation of analytical sedimentation data for proteins. In: Harding, SE.; Rowe, AJ.; Horton, JC., editors. Analytical

Ultracentrifugation in Biochemistry and Polymer Science. Vol. 224. Cambridge, UK: The Royal Society of Chemistry; 1992. p. 90-125.

Liu S, Stafford WF. An optical thermometer for direct measurement of cell temperature in the Beckman instruments XL-A analytical ultracentrifuge. Anal Biochem. 1995; 224(1):199–202. [PubMed: 7710072]

Maurer SP, Bieling P, Cope J, Hoenger A, Surrey T. GTPγS microtubules mimic the growing microtubule end structure recognized by end-binding proteins (EBs). PNAS. 2011; 108(10):3988–3993. [PubMed: 21368119]

Maurer SP, Fourniol FJ, Bohner G, Moores CA, Surrey T. EBs recognize a nucleotide-dependent structural cap at growing microtubule ends. Cell. 2012; 149(2):371–382. [PubMed: 22500803]

Philip JT, Pence CH, Goodson HV. MTBindingSim: simulate protein binding to microtubules. Bioinformatics. 2012; 28(3):441–443. [PubMed: 22171336]

Philo JS. Improved methods for fitting sedimentation coefficient distributions derived by time-derivative techniques. Anal Biochem. 2006; 354(2):238–246. [PubMed: 16730633]

Sandblad L, Busch KE, Tittmann P, Gross H, Brunner D, Hoenger A. The Schizosaccharomyces Pombe EB1 homolog Mal3p binds and stabilizes the microtubule lattice seam. Cell. 2006; 127(7): 1415–1424. [PubMed: 17190604]

Schuck P. Sedimentation analysis of noninteracting and self-associating solutes using numerical solutions to the Lamm equation. Biophys J. 1998; 75(3):1503–1512. [PubMed: 9726952]

Seetapun D, Castle BT, McIntyre AJ, Tran PT, Odde DJ. Estimating the microtubule GTP cap size in vivo. Curr Biol. 2012; 22(18):1681–1687. [PubMed: 22902755]

Simon JR, Salmon ED. The structure of microtubule ends during the elongation and shortening phases of dynamic instability examined by negative-stain electron microscopy. J Cell Sci. 1990; 96(Pt 4): 571–582. [PubMed: 2283357]

Skube S, Chaverri JM, Goodson HV. Effect of GFP tags on the localization of EB1 and EB1 fragments in vivo. Cell Motil Cytoskeleton. 2011; 67(1):1–12.

Slep KC, Vale RD. Structural basis of microtubule plus end tracking by XMAP215, CLIP-170, and EB1. Mol Cell. 2007; 27(6):976–991. [PubMed: 17889670]

Slep KC, Rogers SL, Elliott SL, Ohkura H, Kolodziej P, Vale RD. Structural determinants for EB1-mediated recruitment of APC and spectraplakins to the microtubule plus end. J Cell Biol. 2005; 168(4):587–598. [PubMed: 15699215]

Stafford WF, Sherwood PJ. Analysis of heterologous interacting systems by sedimentation velocity: curve fitting algorithms for estimation of sedimentation coefficients, equilibrium and kinetic constants. Biophys Chem. 2004; 108(1–3):231–243. [PubMed: 15043932]

Sui H, Downing KH. Structural basis of interprotofilament interaction and lateral deformation of microtubules. Structure. 2010; 18(8):1022–1031. [PubMed: 20696402]

Tirnauer JS, Grego S, Salmon ED, Mitchison TJ. EB1 – microtubule interactions in Xenopus egg extracts: role of EB1 in microtubule stabilization and mechanisms of targeting to microtubules. Mol Biol Cell. 2002; 13:3614–3626. [PubMed: 12388761]

Zhu ZC, Gupta JJ, Slabbekoorn AR, Paulson B, Folker ES, Goodson HV. Interactions between EB1 and microtubules: dramatic effect of affinity tags and evidence for cooperative behavior. J Biol Chem. 2009; 284(47):32651–32661. [PubMed: 19778897]

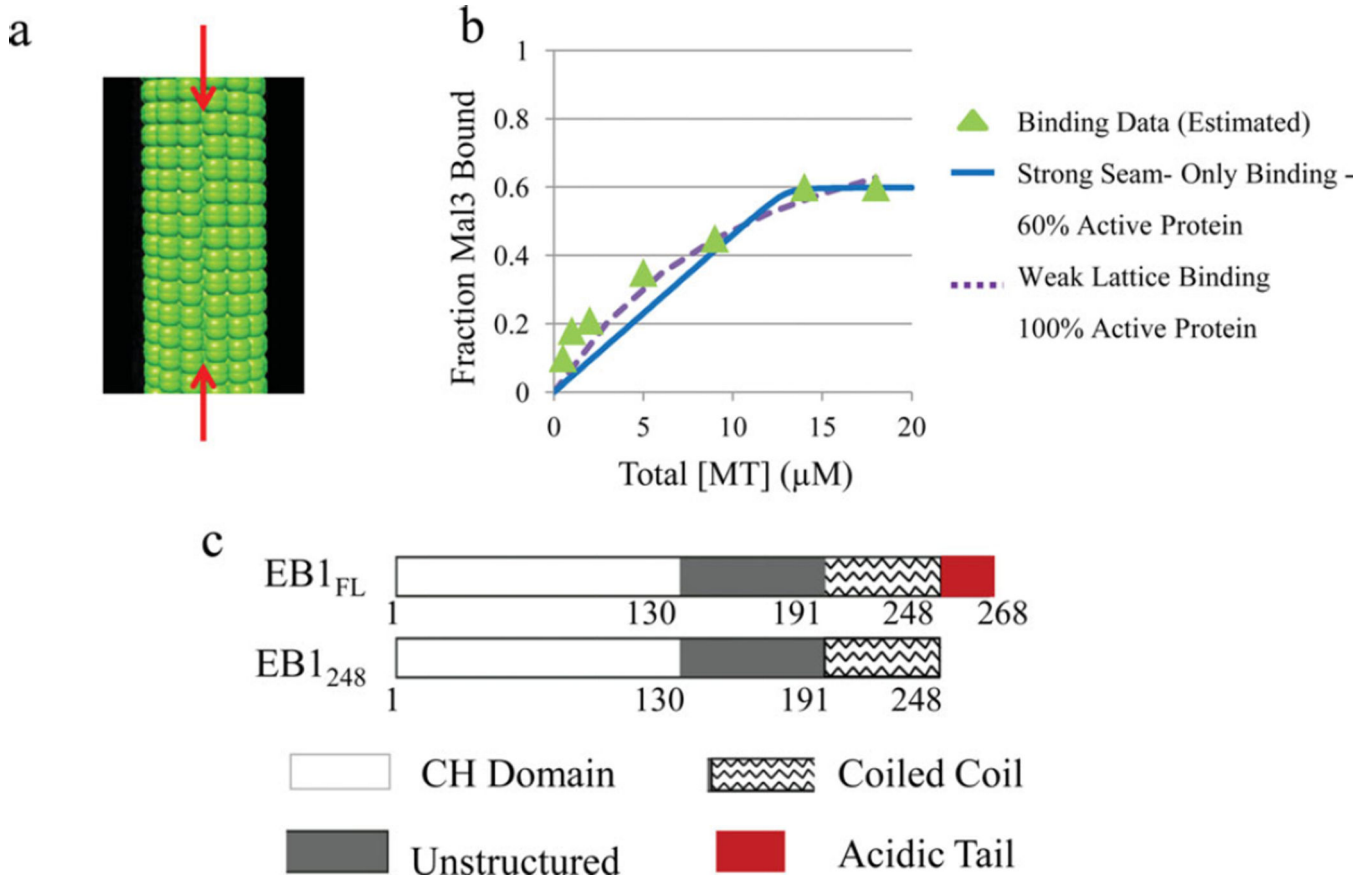

Fig. 1.

(a) MT structure. The image depicts a 13 protofilament MT with the seam at the point of closure (red arrow). The seam is location of the lattice discontinuity where α-tubulin is adjacent to β-tubulin [Desai and Mitchison, 1997]. **(b)** Existing Mal3p-binding data are consistent with multiple binding models. Experimental data (green triangles) for binding of Mal3p (2.3 μM) to MTs (varied as indicated) were extracted from published work [Sandblad et al., 2006] and compared to the behavior expected under the seam-only binding and lattice-binding models. The blue curve (seam-only binding) is a mathematical embodiment of the conceptual model proposed by Sandblad et al. [2006], where Mal3p binds strongly to the seam, and binding of 2.3 μM Mal3p saturates at ~18 μM MTs. Saturation of Mal3p binding at ~18 μM requires that only 60% of the Mal3p is active, and that binding to the seam is very tight (here we used $K_{d\text{-}S}$ = 0.001 μM). The purple curve (lattice binding) shows the predicted behavior of weak lattice binding ($K_{d\text{-}L}$ = 10 μM) with 100% active Mal3p. As can be seen by comparison of the data and curves, each of these models is similarly consistent with these data. Note that in (b) and throughout the manuscript, the data and simulations are presented as a function of total polymerized tubulin instead of free polymerized tubulin because total polymerized tubulin is a known quantity in any experiment, while calculation of free polymerized tubulin would require the assumption of a particular EB1: tubulin binding ratio, and this is unknown in a situation where one is trying to distinguish between seam-only binding and lattice-binding models. **(c)** Schematic diagram of EB1 constructs used in this work. The $EB1_{248}$ fragment lacks the autoinhibitory tail domain and is used in

most of the binding experiments. $EB1_{FL}$ was also tested for whether it preferentially binds to the MT seam or lattice and used to extract an $EB1_{FL}$ dimerization K_d of 90 nM.

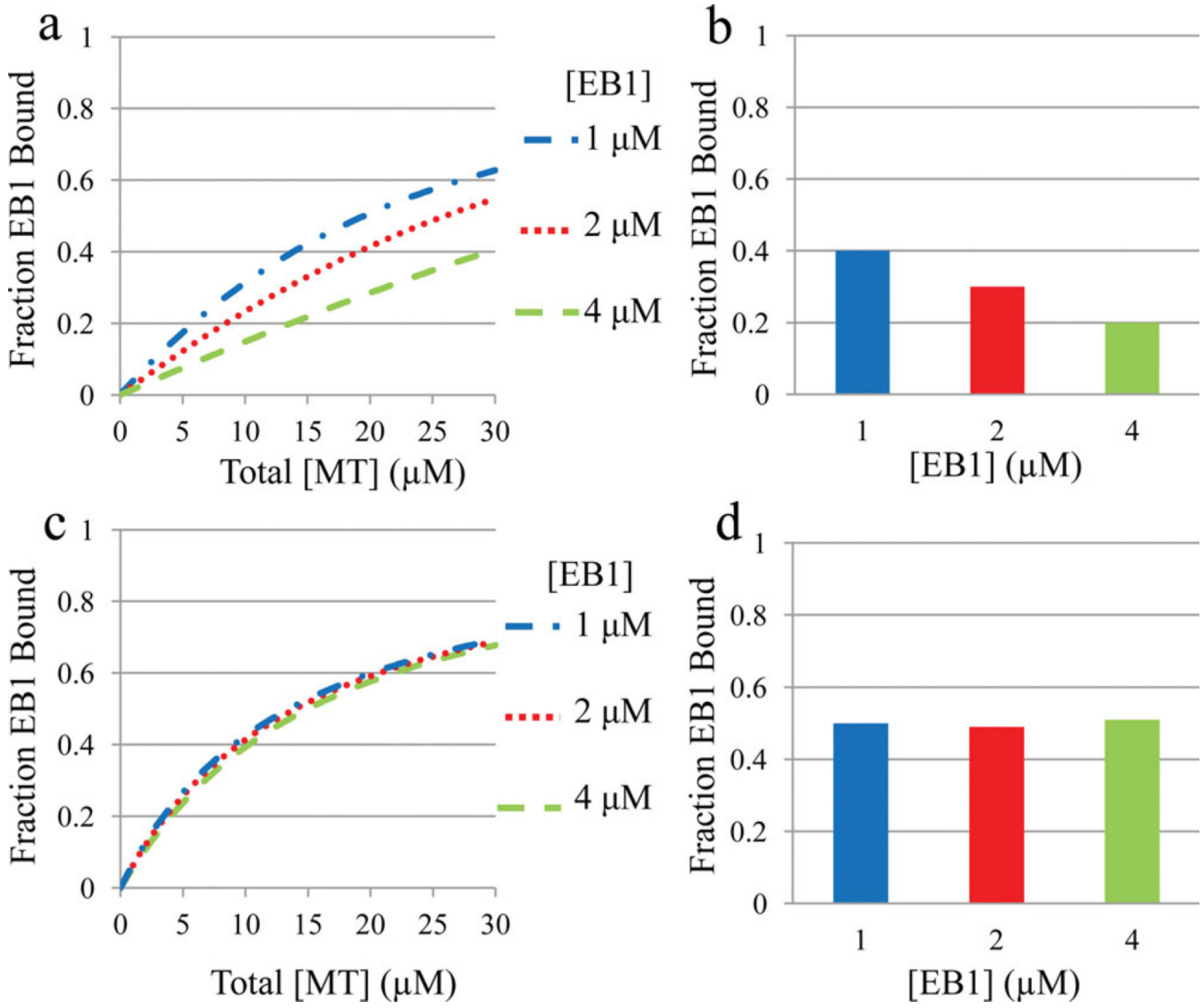

Fig. 2. $EB1_{248}$ cosedimentation behavior predicted from the seam-only binding (a, b) and lattice-binding (c, d) models at different concentrations of EB1

Panels (a) and (c) show the full binding curves predicted by the seam-only ($K_{d\text{-}S}$ = 1 μM) and lattice ($K_{d\text{-}L}$ = 13 μM) binding models respectively, while (b) and (d) show the fraction of $EB1_{248}$ predicted to bind MTs at one particular MT concentration (15 μM). These graphs show that there is a clear distinction between the predicted behaviors of the lattice and seam-only binding models when the concentration of EB1 is shifted between 1 and 4 μM.

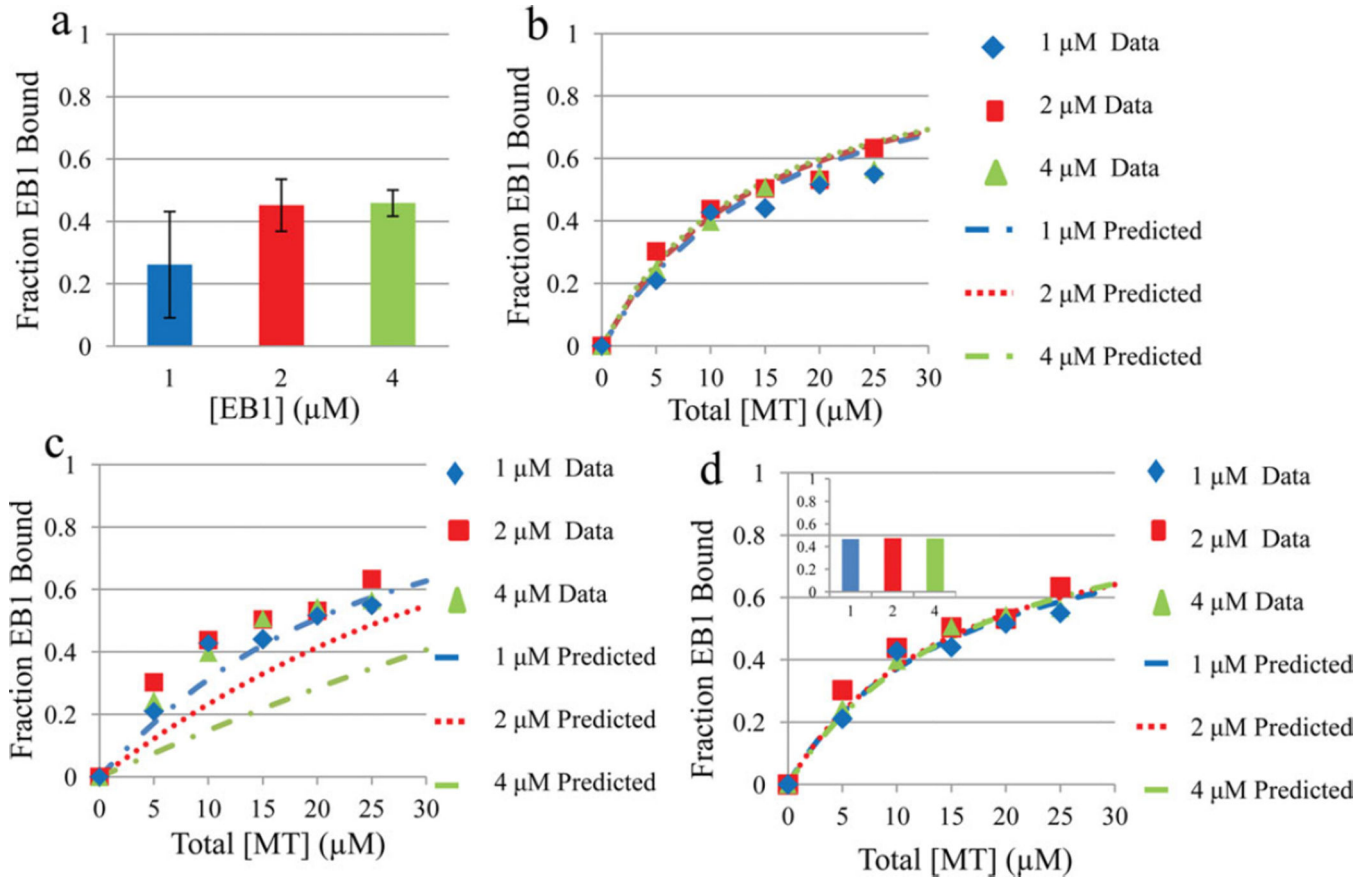

Fig. 3. Comparison of experimental binding data to the predictions of the binding models at different concentrations of $EB1_{248}$

(a) Experimental data showing the fraction of $EB1_{248}$ bound to 15 μM MTs as measured by cosedimentation assays at 1, 2, and 4 μM EB1. These data are inconsistent with the seam-only binding model because the seam-only binding model predicts a decrease in binding fraction as EB1 concentration increases (compare Figs. 3a to 2b and 2d). The 1 μM EB1 apparent deviation from the predictions of the lattice model is not statistically significant as determined by a student's *t*-test. **(b, c)** Experimental data for binding of different concentrations of EB1 to MTs across a range of MT concentrations as compared to the predictions of the lattice-binding model (b) and seam-only binding model (c). Comparison of the data points to the theoretical curves argues strongly against the seam-only binding model for human EB1 and supports the lattice-binding model except that as in 3a, the data for the fractional saturation of 1 μM EB1 are somewhat lower than predicted, though still within the error of the individual measurements. The data points in panels (a–c) are the mean of $n = 3$ experiments, and the error bars in panel (a) are standard deviations. The standard deviations of the data in panels (b) and (c) have been omitted for clarity but are provided in the supplementary data (Supporting Information Figs. S2a–S2c). **(d)** Predicted EB1-binding behavior under a model where EB1 dimerizes. In this model, EB1 dimers bind to the lattice with a K_d of 13 μM (consistent with Fig. 1c), EB1 monomers bind to the lattice with a K_d of 100 μM (as suggested by previous binding experiments [Skube et al., 2011]), and the EB1–EB1 dimerization K_d was set to 90 nM (value obtained from the AUC data).

The inset shows the fraction of EB1 that is predicted to be bound to 15 μM MTs (compare inset to Fig. 3a). Examination of these data show that the dimerization model does not account for the slightly reduced binding of 1 μM EB1 as seen in Figs. 3a–3c, but it does appear to be more consistent with the full data set than is a lattice-binding model that does not account for EB1 monomer-dimer equilibrium (compare Figs. 3d–3b, see also Supporting Information Table S1). The 1 μM deviation could be a result of experimental error or a sign of additional cooperativity as suggested by Zhu et al. [2009].

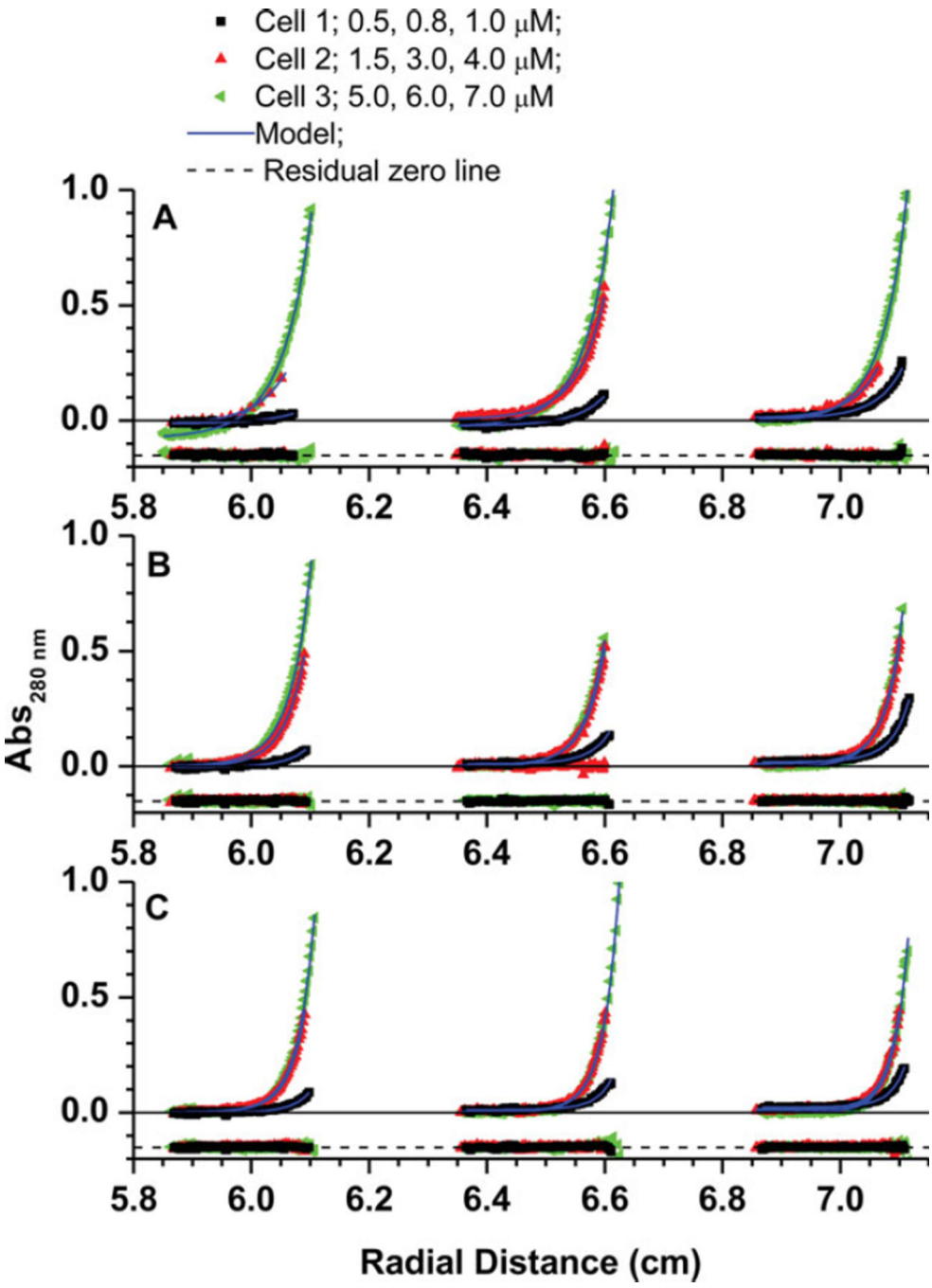

Fig. 4. AUC Sedimentation Equilibrium data collected at 280 nm and 4°C in PEM buffer

In this experiment, the equilibrium distributions for nine samples of $EB1_{FL}$ ranging from 0.5–7.0 μM were measured at three angular velocities at 4°C and globally analyzed. The nine samples were simultaneously run in three SE cells where each cell contains three channels for samples, demonstrated by the different radial distances (i.e., each cell has three channels that begin at 5.85, 6.35, and 6.85 cm, respectively). Cell 1 (black squares) 0.5–1.0 μM, cell 2 (red triangles) 1.5–4.0 μM, and cell 3 (green left-facing triangles) 5.0–7.0 μM. The three panels display the same nine samples at three angular velocities: (**A**) 21,000 rpm,

(**B**) 25,000 rpm, and (**C**) 28,000 rpm. All 27 data sets (nine concentrations at three velocities) were globally fit to a reversible monomer–dimer association model (blue line, Supporting Information Table S2). The difference between the experimental data (black, red and green points) and the model (blue line), or the residuals, is plotted below the line (The residuals have been artificially offset by −0.15 Abs units in order to better visualize the data). The excellent agreement between the model and the experimental data, as demonstrated by the lack of systematic trends in the residuals, indicates that the model accurately explains the data. The model suggests that $EB1_{FL}$ exhibits a reversible dimerization with a K_d of 88.5 nM {24 nM, 196 nM} (best fit {68% confidence interval}).

Table I

Estimated EB1 Concentrations in vivo Reported in the Literature.

Citation	Estimated [EB1]	System
Tirnauer et al. [2002]	0.25 μM	Xenopus egg extract
Katsuki et al. [2009]	"Tens of nanomolar"	*S. pombe*
This work	~0.25 μM	HeLa cytosol
Kronja et al. [2009]	1.5–2.0 μM	Xenopus egg extract

Table I summarizes the estimated EB1 concentration in vivo found in various model systems. The concentration of EB1 in vertebrate cytoplasm has previously been reported as being 0.25 μM and 2 μM in *Xenopus* egg extract [Tirnauer et al., 2002; Kronja et al., 2009] and tens of nanomolar in *S. pombe* [Katsuki et al., 2009]. Using quantitative western blots (Supporting Information Fig. S4), we measured the concentration of EB1 in HeLa cytosol (10.6 mg/ml) to be 0.080 ± 0.004 μM. Assuming that the cytosol is diluted ~3× during preparation, we estimate the concentration of EB1 in HeLa cells to be ~0.25 μM.